Atmos. Chem. Phys. Discuss., 13, 8985–9016, 2013
www.atmos-chem-phys-discuss.net/13/8985/2013/
doi:10.5194/acpd-13-8985-2013

Atmospheric Chemistry and Physics Discussions

Characterization of ultrafine particle number concentration and new particle formation in urban environment of Taipei, Taiwan

H. C. Cheung, C. C.-K. Chou, W.-R. Huang, and C.-Y. Tsai

Research Center for Environmental Changes, Academia Sinica, Taipei 11529, Taiwan

Received: 7 January 2013 – Accepted: 18 March 2013 – Published: 4 April 2013

Correspondence to: C. C.-K. Chou (ckchou@rcec.sinica.edu.tw)

Published by Copernicus Publications on behalf of the European Geosciences Union.

Abstract

An intensive aerosol characterization experiment was performed at the Taipei Aerosol and Radiation Observatory (TARO, 25.02° N, 121.53° E) in the urban area of Taipei, Taiwan during July 2012. Number concentration and size distribution of aerosol particles were measured continuously, which were accompanied by concurrent measurements of mass concentration of submicron particles, PM_1 ($d \leq 1\,\mu m$), and photolysis rate of ozone, $J(O^{1D})$. The averaged number concentrations of total (N_{total}), accumulation mode (N_{acu}), Aitken mode (N_{Aitken}), and nucleation mode (N_{nuc}) particles were $7.6 \times 10^3\,cm^{-3}$, $1.2 \times 10^3\,cm^{-3}$, $4.4 \times 10^3\,cm^{-3}$, and $1.9 \times 10^3\,cm^{-3}$, respectively. Accordingly, the ultrafine particles (UFPs, $d \leq 100\,nm$) accounted for 83 % of the total number concentration of particles measured in this study ($10 \leq d \leq 429\,nm$), indicating the importance of UFPs to the air quality and radiation budget in Taipei and its surrounding areas. An averaged N_{nuc}/NO_x ratio of $\sim 60\,cm^{-3}\,ppbv^{-1}$ was derived from nighttime measurements, which was suggested to be the characteristic of vehicle emissions that contributed to the "urban background" of nucleation mode particles throughout a day. On the contrary, it was found that the number concentration of nucleation mode particles was independent of NO_x and could be elevated up to 10 times the "urban background" levels during daytime, suggesting a substantial amount of nucleation mode particles produced from photochemical processes. Consistency in the time series of the nucleation mode particle concentration and the proxy of H_2SO_4 production, $UVB{\cdot}SO_2$, for new particle formation (NPF) events showed that photo-oxidation of SO_2 was responsible for the formation of new particles in our study area. Moreover, analysis upon the diameter growth rate, GR, and formation rate of nucleation mode particles, J_{10-25}, found that the values of GR ($8.5 \pm 6.8\,nm\,h^{-1}$) in Taipei were comparable to other urban areas, whereas the values of J_{10-25} ($2.2 \pm 1.2\,cm^{-3}\,s^{-1}$) observed in this study were around the low end of the range of new particle formation rate reported by previous investigations. It was revealed that the particle growth rate correlated exponentially with the photolysis of ozone, suggesting the condensable vapors were pro-

ACPD
13, 8985–9016, 2013

duced mostly from photo-oxidation reactions. In addition, this study also revealed that both GR and J_{10-25} exhibited quadratic relationship with the number concentration of particles. The quadratic relationship was inferred as a result of aerosol dynamics and featured NPF process in urban areas.

1 Introduction

Atmospheric particulate matter (PM) is one of the main pollutants impacting air quality and climate. PM interacts with solar radiation which altering the climate forcing directly (Charlson et al., 1992; Myhre, 2009), and plays as cloud condensation nuclei (CCN) to influence the cloud formation processes (Twomey, 1977; Wang and Penner, 2009). PM is also found being able to induce respiratory and cardiovascular diseases when they are breathed in (Nel, 2005).

While the air quality standards have been setup for the mass concentrations of PM_{10} and/or $PM_{2.5}$ (particulate matters with aerodynamic diameters less than 10 or 2.5 µm, respectively), several studies indicated the health effects of ultrafine particles (diameter ≤ 100 nm) and thereby raised public concerns. In contrast to the small mass fraction in PM, UFPs typically account for about two thirds or higher of the total number concentrations of urban particulate matters (Stanier et al., 2004; Woo et al., 2001). They can penetrate deeper into human lung than fine and coarse particles (Churg and Brauer, 2000). Oberdörster and Utell (2002) suggested that UPFs may cross the blood-brain and alveolar-capillary barriers, and enter the central nervous system. Studies have been conducted on the UFPs' impacts on morbidity and mortality (Wichmann et al., 2000), local and regional air quality (Cheung et al., 2012), and their spatiotemporal characteristics and formation processes in urban areas (Cheung et al., 2011; Hussein et al., 2004). Local vehicle exhaust was found to be a major source of UFPs in urban areas (Morawska et al., 2008). Particle number concentration (PNC) was positively related to the traffic volume, where the UFPs number concentrations reached the daily maxima during traffic peak hours (Cheung et al., 2012), and it was affected by the

ACPD
13, 8985–9016, 2013

measurement distance to the sources (Morawska et al., 2008) and wind speed (Hussein et al., 2006). Particle number concentrations from direct emission of diesel engine did not vary significantly under different operating conditions (Kasper, 2005; Ristovski et al., 2006). In addition to the vehicle emissions, UFPs can also be formed by new particle formation (NPF) processes which were frequently observed within urban boundary layer (e.g. Woo et al., 2001; Stanier et al., 2004; Fernández-Camacho et al., 2010; Cheung et al., 2011). Elevated particle number concentrations were found during the new particle formation events associated to photochemical production processes (Cheung et al., 2011, 2012). These studies concluded that the UFPs were contributed from the secondary formation mechanisms as well as from the primary local emissions in an urban environment.

Particle number concentration measurements conducted in urban areas of Taiwan were limited (Chang and Lee, 2007b; Young et al., 2013). Although the relationship between PNC and local vehicle emission was studied, investigation on the influences of secondary formation on PNC was relatively scarce. To better understand the characteristics of PM in terms of number concentration and the factors influencing the NPF in urban environment, we initiated a one month measurement campaign in urban area of Taipei city, Taiwan, during summer 2012. The outcomes of this study are valuable to improving our understandings upon the critical factors governing the NPF under urban setting and formulation of air quality management plan.

2 Methodology

2.1 The topography and meteorology of Taipei region

Taipei metropolis locates in the northern Taiwan with around 6 million inhabitants. As shown in Fig. 1, Taipei is in a topographical basin surrounded by hills of around 500–1000 m in elevation. Wind circulation system of Taipei is governed by the seasonal monsoons that northeasterly flow dominated in winter and southwesterly in summer,

ACPD
13, 8985–9016, 2013

and occasionally accompanied by tropical storms or typhoons. It is dry and stable with poor dispersion conditions as under a high-pressure, but wet and unstable with well dispersion on most days. Air quality of Taipei is mainly influenced by the local emissions, in particular vehicle exhausts. In addition to the local sources, long range transport of air pollutants from the eastern China is also important to the air quality of northern Taiwan during the seasons of winter monsoons, while photochemical production was suggested a key source of fine PM in summertime (Chang and Lee, 2006, 2007a).

2.2 Observation site and instrumentation

The measurements were conducted at the Taipei Aerosol and Radiation Observatory (TARO, 25.02° N, 121.53° E), which locates in the downtown area of Taipei city (Fig. 1), during 4–29 July 2012. The aerosol observatory is on the top floor of the Building-B of the Department of Atmospheric Sciences, National Taiwan University (ASNTU) that is ~20 m a.g.l.

Particle size distribution in the range of 10–429 nm was measured by a Scanning Mobility Particle Sizer (SMPS) system, which consisted of two parts: an Electrostatic Classifier (EC) (Model: TSI 3080, TSI Inc.) and a Condensation Particle Counter (CPC) (Model: TSI 3786, TSI Inc.). The EC was equipped with a long-differential mobility analyzer (long-DMA, Model: TSI 3081, TSI Inc.), which can separate the poly-disperse particles into selected mono-disperse particles according to their electrostatic mobility. The number concentration of the mono-disperse particles was then counted by the CPC. Each ambient sample was drawn into the SMPS system from outside the building through a 0.635 cm (inner diameter) conductive tube and a sampling duration of 5 min was adopted for each particle size distribution measurement. The SMPS system was operated with the sheath and aerosol flow rates of 6 Lpm and 0.6 Lpm, respectively. The system flow rates were checked weekly during the sampling period. Besides, the accuracy of the particle sizing of EC was checked using polystyrene latex spheres before the campaign. Multiple charge correction was applied to the particle size distribu-

ACPD
13, 8985–9016, 2013

tion measurements using the internal algorithm from the Aerosol Instrument Manager Software.

During the study period, continuous measurement of PM_1 (particulate matters with aerodynamic diameters less than 1 µm) mass concentration with time resolution of one hour was also conducted at TARO using a Tapered Element Oscillating Microbalance (TEOM) (Model: TEOM 1405, Thermo Scientific Inc.) equipped with a Filter Dynamics Measurement System (FDMS) and a 1 µm Sharp Cut Cyclon (Model: SCC-2.229, BGI Inc.) at the inlet. Besides, photolysis rate of ozone, $J(O^{1D})$, was measured using an Actinic and Irradiance Spectral Radiometer (Metcon gmbh, Germany). Moreover, to support the data interpretation of pollution sources, the hourly averaged mass concentrations of PM_{10} and $PM_{2.5}$ and the mixing ratios of O_3, CO, NO_x and SO_2 from the Guting air quality station of Taiwan Environmental Protection Agency (Taiwan EPA), which is about 1 km to the TARO, was analyzed in this study. The O_3 was measured using an UV-photometry instrument (Ecotech 9810, with detection limit of 0.5 ppbv and accuracy of ±1 ppb). The oxide of nitrogen (NO_x) was measured using a chemiluminescence analyzer (Ecotech 9841, with detection limit of 0.5 ppbv and accuracy of ±1 % of instrument reading). The CO was detected by a non-dispersive infrared analyzer (Horiba, with detection limit of 50 ppbv and accuracy of ±1 % of full scale), whereas SO_2 was measured by a pulsed UV fluorescence analyzer (Ecotech 9850, with detection limit of 0.5 ppbv and accuracy of ±1 % of instrument reading). Span and zero calibrations for all the gas analyzers were conducted on daily base at all the air quality stations of Taiwan EPA. More details about the measurement techniques and quality control guidelines are referred to the website of Taiwan EPA (http://taqm.epa.gov.tw/taqm/en/default.aspx).

2.3 Data processing and analysis

Particle number concentrations for different size ranges were calculated by the particle size distribution from SMPS measurement. The particle number concentrations were classified into $10 \leq d \leq 429$ nm (N_{total}), $100 \leq d \leq 429$ nm (N_{acu}), $25 \leq d < 100$ nm

ACPD
13, 8985–9016, 2013

(N_{Aitken}) and $d < 25$ nm (N_{nuc}), for total, accumulation mode, Aitken mode and nucleation mode, respectively. For graph plotting, time resolution of 5 min was used for particle data, whereas the data for trace gases and meteorological parameters were hourly based. Thus the 5 min particle number concentration and size distribution data were then calculated into hourly averages for data comparison and analysis purposes. Pearson coefficient, r, was calculated by *PASW Statistics ver. 18* (SPSS Inc.) to determine the correlation among the parameters. The back-trajectories of air masses were calculated using the HYSPLIT model of NOAA (National Oceanic and Atmospheric Administration) (Draxler 1999).

3 Results and discussion

3.1 General description of weather conditions during measurement periods

Backward trajectories were calculated for the TARO during the sampling period. During the early period of the campaign, southwesterly winds were found to prevail (from 4–19 July) under the influence of summer monsoons (see Fig. 2a). For the later period (from 20–27 July), easterly winds were dominating for the influences of the cyclonic system developed nearby the southern Taiwan (see Fig. 2b). Showers were occasionally observed in the afternoon during the sampling period.

3.2 Overall statistics of particle measurement

Statistics of particle number and mass concentrations are shown in Table 1. The overall N_{total}, N_{acu}, N_{Aitken} and N_{nuc} were found to be 7.6×10^3 cm^{-3}, 1.2×10^3 cm^{-3}, 4.4×10^3 cm^{-3}, 1.9×10^3 cm^{-3}, respectively. The N_{total} was comparable to urban areas including Brisbane, Australia (9.3×10^3 cm^{-3}, Cheung et al., 2011); Helsinki, Finland (10×10^3 cm^{-3}, Hussein et al., 2004), but lower than that of the more polluted urban areas in Yangtze River Delta, China (Gao et al., 2009), Barcelona, Spain (Pey et al.,

ACPD
13, 8985–9016, 2013

2008) and Atlanta, United States (Woo et al., 2001), which reached above the magnitude of 10^4 cm^{-3}. Furthermore, the N_{total} measured at urban area of northern Taiwan in the current study was significantly lower than that observed over urban central Taiwan, which was 3.8×10^4 cm^{-3} during the summertime (Young et al., 2012). Note that, in the latter study, NPF events occurred almost every day during the study period due to the presence of numerous industrial emission sources in that study region, which were suggested to induce a significantly higher PNC.

The particle mass concentrations of PM_{10}, $PM_{2.5}$ and PM_1 were 39.6 µg m^{-3}, 21.6 µg m^{-3}, and 10.3 µg m^{-3}, respectively, for the entire sampling period. The number and mass concentrations of particles were found to be significantly lower under the influence of the cyclonic system. For example, the averaged PM_1 and N_{total} were 3.5 µg m^{-3} and 3.3×10^3 cm^{-3} under the influence of the cyclonic system, while 12.6 µg m^{-3} and 9.5×10^3 cm^{-3} were obtained for other days. The lower particle concentrations were suggested due to the stronger atmospheric dispersion associated to the cyclonic system. Relatively higher wind speed was measured during this period which was 3.4 m s^{-1}, compared to 1.9 m s^{-1} for other days. In addition to the dispersion, strong surface winds can affect two particle dynamic processes: condensation of semivolatile gases and coagulation among the freshly formed particles and/or the existing aerosol particles.

3.3 Relationship between PNC and other parameters

Relationship between PNC and other parameters were further assessed in this section. Pearson correlation coefficients, r, were calculated between PNC and particle mass concentrations, primary gaseous pollutants (including CO, NO_x, and SO_2) and meteorological parameters (wind speed, relative humidity and temperature). In general, PNC does not show a strong correlation against mass concentrations. For example, the r value between $PM_{2.5}$ and N_{nuc} was found to be 0.34 ($p < 0.05$). However, the pattern of scatterplots between PNC and $PM_{2.5}$ suggested that the particles observed at the

ACPD
13, 8985–9016, 2013

TARO could be contributed from two groups of pollution sources during summer period (see Fig. 3a–c). A linear relationship was found to be dominant for the group A; on the other hand, higher N_{nuc} was observed for the group B while $PM_{2.5}$ was varying around 10–30 $\mu g\,m^{-3}$.

Vehicle exhaust emission was suggested to be a major source contributing the group A pollution which is always present in urban environment. On the other hand, NPF events were observed only during daytime in this study. Therefore, we separate the data into daytime (08:00–15:59 LT) and nighttime (20:00–03:59 LT) to better examine the relationship between N_{nuc} and vehicle exhaust emission. The mixing ratio of NO_x was used as an indicator of the vehicle emission in urban environment and scatterplots between N_{nuc} and NO_x were done for the daytime and nighttime data, respectively.

For the nighttime data (see Fig. 4a), a good linear correlation between N_{nuc} and NO_x was obtained ($r = 0.78$, $p < 0.05$), indicating that about 60 cm^{-3} nucleation mode particles were emitted with a unit of NO_x (in ppbv) where vehicle exhaust emission dominated. Note that this emission ratio was applicable only for the study area, since it would depend on the local emission properties (i.e. types of fuel and vehicles) and the meteorological conditions. Figure 4b shows the daytime data of N_{nuc} against NO_x with a line fit obtained from Fig. 4a to represent an emission ratio of primary pollution. Note that, at times, the daytime N_{nuc} was enhanced up to 10 times the level estimated by the N_{nuc}/NO_x emission ratio. The results suggest that, in the budget of N_{nuc} of urban Taipei, the primary (NO_x relevant) sources contributed throughout a day, whereas the other (NO_x independent) sources dominated during daytimes, in particular during the episodes of new particle burst. Previous studies of NPF events in urban areas showed that the burst of nucleation mode particles was associated strongly with photochemical production of sulfuric acid (Woo et al., 2001; Stanier et al., 2004; Cheung et al., 2012). Similar finding has been reported in other polluted urban area of central Taiwan (Young et al., 2012). The discussion on the NPF will be provided in the following sections.

ACPD
13, 8985–9016, 2013

3.4 Observation of new particle formation

A NPF event is defined as the increase of the number concentration of nucleation mode particles, and those particles are growing into Aitken and/or accumulation modes size range (≥ 25 nm) and last for a few hours until its disappear in atmosphere by condensation/coagulation sinks (Dal Maso et al., 2005). Averaged diurnal variations of N_{total}, N_{acu}, N_{nuc} and the UVB for this study are depicted in Fig. 5. Two peaks were observed for N_{total} at 11:00 LT and 18:00 LT. The first one was most likely contributed by NPF which was associated with daily maxima of UVB, and the second peak suggested the influence of traffic emission in late afternoon. We then separate the N_{total} into two groups, (i) N_{nuc} and (ii) N_{acu} for nucleation and accumulation mode particles, respectively, in further analysis. A mode of N_{nuc} was observed near 10:00 LT and the peak of N_{acu} was observed one hour later. This suggested that nucleation mode particles were formed in the morning where particles have subsequently grown into larger sizes (Cheung et al., 2011).

During the study period, a total of nine NPF events were observed. NPF events occurred frequently in the period from 8 July to 19 July (eight events in twelve days) and on 27 July. Figure 6 shows the time series of particle size distribution (lower panel), N_{total} (middle panel) and wind direction/speed (upper panel) for the entire campaign period. The general meteorological conditions for the NPF events were sunny day with southwesterly to northwesterly winds during initial stage of the events. The averaged daytime (08:00–16:00 LT) wind speeds for NPF-event and non-event days were 2.61 ms^{-1} ($\pm$0.43 ms^{-1}) and 3.23 ms^{-1} ($\pm$1.45 ms^{-1}), respectively. The relatively lower and lesser fluctuation wind speed on NPF days implied a stable atmospheric condition setting favorable for the new particle formation. Higher mean N_{total} and N_{nuc} were found to be 9.4×10^3 cm^{-3} and 2.4×10^3 cm^{-3} for NPF event days compared to that for non-event days (N_{total}: 6.1×10^3 cm^{-3} and N_{nuc}: 1.6×10^3 cm^{-3}, see Table 2). Also the 95th percentile of N_{nuc} (8.1×10^3 cm^{-3}) during the NPF event reached nearly one fold of that measured on non-event days. These results suggested that the burst of nucleation

ACPD
13, 8985–9016, 2013

mode particles induced by the NPF had caused a significant impact on local air quality during this campaign period.

During the NPF events, the variation of N_{nuc} was found to be coincident with that of UVB·SO_2, an index of photochemical production of ambient H_2SO_4. Figure 7 shows the time series of N_{nuc} and UVB·SO_2 (upper panel) and the particle size distributions from 8–14 July during which consecutive nucleation events were observed. The variations of N_{nuc} and UVB·SO_2 were qualitatively agreed. The increases of the N_{nuc} during the NPF events were also contributed by other sources, for example the local vehicle emission which mentioned in previous Sect. 3.3. Nevertheless, this result suggested that H_2SO_4 was playing an important role for the particle formation process in our study region.

We further investigated the sources of SO_2 influencing the NPF around Taipei city. Figure 8 shows averaged SO_2 mixing ratios over Taipei region during the study period (only daytime 08:00–15:59 LT was used). The results showed that two hot spots were observed with relatively higher SO_2 levels which located at (i) the East Rim of Taipei basin, and (ii) the Southwest of Taipei basin. Truck emission is most likely the major source responsible for the eastern SO_2 hot spot; however, the plumes from the coal fire power plant that locating at the northeastern Taiwan were also suspect. Industrial and vehicle exhaust emissions (diesel engine vehicles) were major sources of SO_2 for western Taipei. Land and sea breeze is a synoptic wind pattern affecting the Taipei City, with south-westerly/westerly winds dominating in the morning, and the wind direction shifted clock-wisely to easterly in afternoon. In the Supplement of this paper, Fig. S1 shows the hourly contour plots of SO_2 (from 07:00 to 12:00 LT) over Taipei region during the NPF event on 8 July 2012. A relatively high SO_2 (~ 10 ppb) was observed in western Taipei, while below 2 ppb of SO_2 was found around TARO, central Taipei, at 07:00 LT. During the morning of 8 July, westerly wind was dominating which could bring the SO_2 plume to the TARO. The observation found NPF event initiated at 11:00 LT, when the SO_2 reached to the daily maxima, 5 ppb. The characteristics in winds and SO_2 described above hold for most of the NPF events except the case on 27 July 2012, where easterly winds dominated with elevated SO_2 in east of TARO at around 09:00–

ACPD
13, 8985–9016, 2013

10:00 LT (see Fig. S2). From these cases, we can see that the transport of SO_2 from the sources around Taipei has substantial impacts upon particle formation process and, thereby, the number concentration UFPs in urban Taipei.

3.5 Growth and formation rates

Table 3 summarizes the averaged growth rate (GR) and formation rate of nucleation mode particles (J_{10-25}), and relevant measurements for respective nucleation events observed in this study. The averaged GR was found to be $8.5 \pm 6.8\,nm\,h^{-1}$ (ranged from 3.3 to $25.5\,nm\,h^{-1}$). The average and range of GR values are similar to previous urban study in Taiwan, which was $11.8\,nm\,h^{-1}$ and ranged from 6.7 to $23.9\,nm\,h^{-1}$, respectively (Young et al., 2013), and are comparable to urban areas of Atlanta, United States with averaged GR of $9.3\,nm\,h^{-1}$ (Stolzenburg et al., 2005) and Beijing, China with averaged GR of $6.0\,nm\,h^{-1}$ (Zhang et al., 2011). Previous studies suggested that the variation of GR values was associated with the meteorological conditions (e.g. temperature, RH) and the presence of condensation vapors (Cheung et al., 2011; Yli-Juuti et al., 2011). Given the persistent emissions of hydrocarbons and SO_2 from local sources in urban Taipei, the production of condensable vapors, either organics or sulfuric acid, was very likely dominated by the availability of hydroxyl radical. Figure 9 illustrates the correlation between GR and the product of $J(O^{1D})$ and mixing ratio of ozone, which gives the production rate of OH radicals from ozone photolysis. It was revealed that the value of GR increased exponentially with photolysis of ozone and in turn the production of OH radicals. The outlier shown in Fig. 9 is for the event on 11 July. The causes of that discrepancy are yet unclear; nevertheless, preliminary investigation suggested that the growth of particle could have been inhibited by stronger winds during that morning (shown in Fig. S3). The significant correlation between GR and OH production warrants that the growth of newly formed particles was driven by photochemical reactions. Moreover, the exponential relationship suggests that the GR could be very sensitive to

ACPD
13, 8985–9016, 2013

the changes in OH production and necessitate further studies on the photochemical dynamics.

Averaged formation rate of nucleation mode particles (J_{10-25}) for each NPF event was calculated for the particles size ranged from ~ 10 to 25 nm according to the method of Dal Maso et al. (2005). Formation rate is defined as sum of the apparent formation rate (dN_{nuc}/dt) and the coagulation loss rate during the NPF event. The mean J_{10-25} for the new particle events was found to be $2.2 \pm 1.2\,cm^{-3}\,s^{-1}$ with the consideration of the coagulation loss. The J_{10-25} observed in this study ranged from 0.6 to $4.8\,cm^{-3}\,s^{-1}$, which is close to the lower limit of the reported formation rates (Kulmala et al., 2004) but comparable to a recent observation for NPF in urban Beijing, China (Yue et al., 2010). The formation rate depends on the chemistry conditions of the atmosphere which induce differences in the formation rates among the respective regions. In this study, the formation rate was influenced by the regional and local (both primary and secondary) sources, also the relatively high level of pre-existing particles could have weakened the nucleation process and lowered the formation rates. Figure 10a shows the relationship between J_{10-25} and the total as well as the nucleation mode PNCs, N_{total} and N_{nuc}, for the NPF events in this study. Apparently, N_{total} increased linearly ($R^2 = 0.6759$) with J_{10-25} to respond the production of new particles during a NPF event. However, N_{nuc} behaved as a quadratic function and reached the maximal level around $1 \times 10^4\,cm^{-3}$ with J_{10-25} ~$3\,cm^{-3}\,s^{-1}$. The differences between N_{total} and N_{nuc} indicated that the newly formed nucleation mode particles have grown rapidly beyond 25 nm in case of high PNC. The dependence of GR to N_{total} is also depicted with quadratic curve-fitting as shown in Fig. 10b. In contrast to the formation rate, GR decreased with N_{total} and reached a minimal around $N_{total} = 1.8 \times 10^4\,cm^{-3}$. The measurements suggested that the GR of particles decreased with the increases in N_{total} because of the increases in the surface area for the condensation of vapors. Interpretation of the turn-up of GR with N_{total} is very uncertain because there was only a single measurement to support it. Nevertheless, given that when the number concentration of particles increased the collision between particles would be enhanced as well, the drastic increase in GR is likely

ACPD
13, 8985–9016, 2013

a result of coagulation instead of condensation. In this context, the difference between N_{total} and N_{nuc} shown in Fig. 10a was also likely a result of enhancement in the coagulation of aerosol particles that could have retarded the accumulation of nucleation mode particles.

4 Conclusions

In this study, an intensive measurement campaign of particle number concentration, size distribution, and mass concentrations was conducted at an urban aerosol observatory (TARO) in Taipei, Taiwan during July 2012. The results indicated that the particle number concentration of the study region was influenced primarily by the local vehicle emissions and the photochemical production in addition to the meteorological conditions. Campaign averages of particle number concentrations N_{total}, N_{acu}, N_{Aitken}, and N_{nuc} were $7.6 \times 10^3\,cm^{-3}$, $1.2 \times 10^3\,cm^{-3}$, $4.4 \times 10^3\,cm^{-3}$, and $1.9 \times 10^3\,cm^{-3}$, respectively. The UFPs (i.e. $N_{Aitken} + N_{nuc}$) accounted for 83 % of the total number concentration of particles measured in this study ($10 \leq d \leq 429$ nm), indicating the importance of UFPs to the air quality and radiation budget in Taipei and its surrounding areas.

An averaged N_{nuc}/NO_x ratio of $\sim 60\,cm^{-3}\,ppbv^{-1}$ was obtained from nighttime measurements, which was suggested to be the characteristic of vehicle emissions and was considered as the "urban background" of nucleation mode particles emitted from primary sources in this study area. Daytime measurements found that the number concentration of nucleation mode particles was elevated up to 10 times the "urban background" levels during NPF events, implying that the formation of new particles was driven by photochemical reactions.

In total nine NPF events were observed during the experiment period; eight of them were under typical land-sea breeze circulation and one event was under the influence of easterly winds. Elevated particle number concentrations were observed during the NPF events with average values of $9.4 \times 10^3\,cm^{-3}$ (N_{total}), compared to $6.1 \times 10^3\,cm^{-3}$ (N_{total}) for the non-event days. All the NPF events were found being associated with

ACPD
13, 8985–9016, 2013

SO_2 advection. The variations in the number concentration of nucleation mode particles and the estimated H_2SO_4 proxy, $UVB \cdot SO_2$, were well agreed during the NPF events, suggesting that oxidation of SO_2 was responsible for the NPF events. There was no NPF event observed at TARO as Taiwan was under the influences of cyclonic system during the measurement period, which was most likely due to enhanced atmospheric dispersion induced by the higher wind speed that suppressed the NPF occurrence.

Growth and formation rates of nucleation mode particles were retrieved from the size distribution measurements. The averages of GR and J_{10-25} for the NPF events observed in this study were $8.5 \pm 6.8\,nm\,h^{-1}$ and $2.2 \pm 1.2\,cm^{-3}\,s^{-1}$, respectively. The range of GR is comparable to the results of previous investigations on urban aerosols, whereas the values of J_{10-25} are close to the low end of the range of new particle formation rate documented in literatures. Analysis on the correlation between GR and the photolysis of ozone revealed that GR increased exponentially with the production of OH radicals, suggesting that the growth of nano-particles was dominated by the production of semi-volatile species from photo-oxidation. Unfortunately, without measurements of the composition of aerosols and precursor gases, the species responsible for the growth of aerosols remain unclear.

Besides the OH production, the values of GR were found to depend on the number concentration of particles as a quadratic function. It was inferred that the GR was dominated by the availability of surface areas for vapor condensation and thereby declined with increases in N_{total}, whereas the coagulation could have enhanced the GR and resulted in the drastic increases in GR in the regime of $N_{total} > 2 \times 10^4\,cm^{-3}$ in our case. The total PNC (N_{total}) was found to be correlated linearly with the new particle formation rate (J_{10-25}), whereas the nucleation mode PNC (N_{nuc}) exhibited as a quadratic function with the maximal level around $1 \times 10^4\,cm^{-3}$ at $J_{10-25} \sim 3\,cm^{-3}\,s^{-1}$. The differences between N_{total} and N_{nuc} indicated that the newly formed nucleation mode particles have grown rapidly beyond 25 nm in case of high PNC, which is typical in urban atmosphere.

ACPD
13, 8985–9016, 2013

Supplementary material related to this article is available online at: http://www.atmos-chem-phys-discuss.net/13/8985/2013/acpd-13-8985-2013-supplement.pdf.

Acknowledgements. The authors gratefully acknowledge the logistic supports from the department of atmospheric sciences, National Taiwan University, and the financial support from the Academia Sinica and the National Science Council through grants 99–2111-M-001-005-MY3 and 100-2111-M-001-003. Also we thank the Taiwan EPA to provide the trace gases and meteorological data.

References

Chang, S.-C. and Lee, C.-T.: Evaluation of the trend of air quality in Taipei, Taiwan from 1994 to 2003, Environ. Monit. Assess., 127, 87–96, 2007a.

Chang, S.-C. and Lee, C.-T.: Secondary aerosol formation through photochemical reactions estimated by using air quality monitoring data in Taipei City from 1994 to 2003, Atmos. Environ., 41, 4002–4017, 2007b.

Charlson, R. J., Schwartz, S. E., Hales, J. M., Cess, R. D., Coakley Jr., J. A., Hansen, J. E., and Hofmann, D. J.: Climate forcing by anthropogenic aerosols, Science, 255, 423–430, 1992.

Chen, J.-P., Tsai, T.-S., and Liu, S.-C.: Aerosol nucleation spikes in the planetary boundary layer, Atmos. Chem. Phys., 11, 7171–7184, doi:10.5194/acp-11-7171-2011, 2011.

Chen, S.-C., Tsai, C.-J., Chou, C. C.-K., Roam, G.-D., Cheng, S.-S., and Wang, Y.-N.: Ultrafine particles at three different sampling locations in Taiwan, Atmos. Environ., 44, 533–540, 2010.

Cheng, Y.-H., Huang, C.-H., Huang, H.-L., and Tsai, C.-J.: Concentrations of ultrafine particles at a highway toll collection booth and exposure implications for toll collectors, Sci. Total Environ., 409, 364–369, 2010a.

Cheng, Y.-H., Liu, Z.-S., and Chen, C.-C.: On-road measurements of ultrafine particle concentration profiles and their size distributions inside the longest highway tunnel in Southeast Asia, Atmos. Environ., 44, 763–772, 2010b.

ACPD
13, 8985–9016, 2013

Cheung, H. C., Morawska, L., and Ristovski, Z. D.: Observation of new particle formation in subtropical urban environment, Atmos. Chem. Phys., 11, 3823–3833, doi:10.5194/acp-11-3823-2011, 2011.

Cheung, H. C., Morawska, L., Ristovski, Z. D., and Wainwright, D.: Influence of medium range transport of particles from nucleation burst on particle number concentration within the urban airshed, Atmos. Chem. Phys., 12, 4951–4962, doi:10.5194/acp-12-4951-2012, 2012.

Churg, A. and Brauer, M.: Ambient atmospheric particles in the airways of human lungs, Ultrastruct. Pathol., 24, 353–361, 2000.

Dal Maso, M., Kulmala, M., Riipinen, I., Wagner, R., Hussien, T., Aalto, P. P., and Lehtinen, K. E. J.: Formation and growth of fresh atmospheric aerosols: eight years of aerosol size distribution data from SMEAR II, Hyytiälä, Finland, Boreal Environ. Res., 10, 323–336, 2005.

Draxler, R. R.: HYSPLIT4 user's guide, NOAA Tech. Memo, ERLARL-230, NOAA Air Resources Laboratory, Silver Spring, MD, 1999.

Fernández-Camacho, R., Rodríguez, S., de la Rosa, J., Sánchez de la Campa, A. M., Viana, M., Alastuey, A., and Querol, X.: Ultrafine particle formation in the inland sea breeze airflow in Southwest Europe, Atmos. Chem. Phys., 10, 9615–9630, doi:10.5194/acp-10-9615-2010, 2010.

Gao, J., Wang, T., Zhou, X., Wu, U., and Wang, W.: Measurement of aerosol number size distributions in the Yangtze River Delta in China: formation and growth of particles under polluted conditions, Atmos. Environ., 43, 829–836, 2009.

Hussein, T., Puustinen, A., Aalto, P. P., Mäkelä, J. M., Hämeri, K., and Kulmala, M.: Urban aerosol number size distributions, Atmos. Chem. Phys., 4, 391–411, doi:10.5194/acp-4-391-2004, 2004.

Hussein, T., Karppinen, A., Kukkonen, J., Harkonen, J., Aalto, P. P., Hämeri, K., Kerminen, V.-M., and Kulmala, M.: Meteorological dependence of size-fractionated number concentrations of urban aerosol particles, Atmos. Environ., 40, 1427–1440, 2006.

Hussein, T., Martikainen, J., Junninen, H., Sogacheva, L., Wagner, R., Dal Maso, M., Riipinen, I., Aalto, P. P., and Kulmala, M.: Observation of regional new particle formation in the urban atmosphere, Tellus B, 60, 509–521, 2008.

Kasper, M.: Sampling and Measurement of Nanoparticle Emissions for Type Approval and Field Control. SAE Tech. Pap. Ser. 2005-26-013, doi:10.4271/2005-26-013, 2005.

ACPD
13, 8985–9016, 2013

Kulmala, M., Vehkamaki, H., Petäjä, T., Dal Maso, M., Lauri, A., Kerminen, V.-M., Birmili, W., and McMurry, P. H.: Formation and growth rates of ultrafine atmospheric particles: a review of observations, Aerosol Sci., 35, 143–176, 2004.

Morawska, L., Moore, M. R., and Ristovski, Z. D.: Health Impacts of Ultrafine Particles: Desktop Literature Review and Analysis, Australian Department of the Environment and Heritage, Canberra, Australia, 2004.

Morawska, L., Ristovski, Z., Jayaratne, E. R., Keogh, D. U., and Ling, X.: Ambient nano and ultrafine particles from motor vehicle emissions: characteristics, ambient processing and implications on human exposure, Atmos. Environ., 42, 8113–8138, 2008.

Myhre, G.: Consistency between satellite-derived and modeled estimates of the direct aerosol effect, Science, 35, 287–190, 2009.

Nel, A.: Air pollution-related illness: Effects of particle, Science, 308, 804–806, 2005.

Oberdörster, G. and Utell, M. J.: Ultrafine particle in the urban air: to the respiratory tract – and beyond?, Environ. Health Persp., 110, A440–A441, 2002.

Pey, J., Rodriguez, S., Querol, X., Alastuey, A., Moreno, T., Putaud, J. P., and Van Dingenen, R.: Variations of urban aerosols in the western Mediterranean, Atmos. Environ., 42, 9052–9062, 2008.

Ristovski, Z., Jayaratne, E. R., Lim, M., Ayoko, G. A., and Morawska, L.: Influence of diesel fuel sulphur on the nanoparticle emissions from city buses, Environ. Sci. Technol., 40, 1314–1320, 2006.

Stanier, C., Khlystov, A., and Pandis, S.: Ambient aerosol size distributions and number concentrations measured during the Pittsburgh Air Quality Study (PAQS), Atmos. Environ., 38, 3275–3284, 2004.

Stolzenburg, M. R., McMurry, P. H., Sakurai, H., Smith, J. N., Mauldin, III, R. L., Eisele, F. L., and Clement, C. F.: Growth rates of freshly nucleated atmospheric particles in Atlanta, J. Geophys. Res., 110, D22S05, doi:10.1029/2005JD005935, 2005.

Twomey, S.: The influence of Pollution on the Shortwave Albedo of Clouds, J. Atmos. Sci., 34, 1149–1152, 1977.

Wang, M. and Penner, J. E.: Aerosol indirect forcing in a global model with particle nucleation, Atmos. Chem. Phys., 9, 239–260, doi:10.5194/acp-9-239-2009, 2009.

Wichmann, H. E., Spix, C., Tuch, T., Wölke, G., Peters, A., Heinrich, J., Kreyling, W. G., and Heyder, J.: Daily mortality and fine and ultrafine particles in Erfurt, Germany part I: role of particle number and particle mass, Res. Rep. Health Eff. Inst., 98, 5–86, 2000.

ACPD
13, 8985–9016, 2013

Woo, K. S., Chen, D. R., Pui, D. Y. H., and McMurry, P. H.: Measurement of Atlanta aerosol size distribution: observation of ultrafine particle events, Aerosol Sci. Technol., 34, 75–87, 2001.

Yli-Juuti, T., Nieminen, T., Hirsikko, A., Aalto, P. P., Asmi, E., Hõrrak, U., Manninen, H. E., Patokoski, J., Dal Maso, M., Petäjä, T., Rinne, J., Kulmala, M., and Riipinen, I.: Growth rates of nucleation mode particles in Hyytiälä during 2003–2009: variation with particle size, season, data analysis method and ambient conditions, Atmos. Chem. Phys., 11, 12865–12886, doi:10.5194/acp-11-12865-2011, 2011.

Young, L.-H., Wang, Y.-T., Hsu, H.-C., Lin, C.-H., Liou, Y.-J., Lai, Y.-C., Lin, Y.-H., Chang, W.-L., Chiang, H.-L., and Cheng, M.-T.: Spatiotemporal variability of submicrometer particle number size distribution in an air quality management district, Sci. Total Environ., 425, 135–145, 2012.

Young, L.-H., Lee, S.-H., Kanawade, V. P., Hsiao, T.-C., Lee, Y. L., Hwang, B.-F., Liou, Y.-J., Hsu, H.-T., and Tsai, P.-J.: New particle growth and shrinkage observed in subtropical environments, Atmos. Chem. Phys., 13, 547–564, doi:10.5194/acp-13-547-2013, 2013.

Yue, D. L., Hu, M., Zhang, R. Y., Wang, Z. B., Zheng, J., Wu, Z. J., Wiedensohler, A., He, L. Y., Huang, X. F., and Zhu, T.: The roles of sulfuric acid in new particle formation and growth in the mega-city of Beijing, Atmos. Chem. Phys., 10, 4953–4960, doi:10.5194/acp-10-4953-2010, 2010.

Zhang, Y. M., Zhang, X. Y., Sun, J. Y., Lin, W. L., Gong, S. L., Shen, X. J., and Yang, S.: Characterization of new particle and secondary aerosol formation during summertime in Beijing, China, Tellus B, 63, 382–394, 2011.

ACPD
13, 8985–9016, 2013

Table 1. Statistic of particle mass and number concentrations measured. Units: PM_{10}, $PM_{2.5}$ and PM_1 in $\mu g\,m^{-3}$; and for N_{total}, N_{acu}, N_{Aitken} and N_{nuc} in cm^{-3}. Note: $PM_{2.5}$ measurement interrupted during the cyclonic period.

	Parameters	Average	Median	S.D.	No. of data
Whole period: 4–29 Jul 2012	PM_{10}	39.6	36.0	15.0	620
	$PM_{2.5}$	21.6	21.0	9.8	403
	PM_1	10.3	9.9	7.0	539
	N_{total}	7.56×10^3	4.55×10^3	7.00×10^3	603
	N_{acu}	1.18×10^3	1.03×10^3	1.00×10^3	603
	N_{Aitken}	4.43×10^3	2.42×10^3	4.72×10^3	603
	N_{nuc}	1.95×10^3	1.20×10^3	2.17×10^3	603
4–19 Jul, and 28–29 Jul 2012	PM_{10}	44.1	42.0	14.3	429
	$PM_{2.5}$	21.8	21.0	9.8	393
	PM_1	12.6	11.9	6.5	403
	N_{total}	9.54×10^3	7.39×10^3	7.28×10^3	412
	N_{acu}	1.57×10^3	1.45×10^3	0.97×10^3	412
	N_{Aitken}	5.66×10^3	4.06×10^3	5.03×10^3	412
	N_{nuc}	2.31×10^3	1.47×10^3	2.40×10^3	412
Cyclonic period: 20–27 Jul 2012	PM_{10}	29.5	28.0	11.1	191
	$PM_{2.5}$	14.7	14.5	6.6	10
	PM_1	3.5	2.8	3.0	136
	N_{total}	3.28×10^3	2.19×10^3	3.65×10^3	191
	N_{acu}	0.34×10^3	0.24×10^3	0.30×10^3	191
	N_{Aitken}	1.78×10^3	1.12×10^3	2.34×10^3	191
	N_{nuc}	1.17×10^3	0.87×10^3	1.21×10^3	191

ACPD
13, 8985–9016, 2013

Table 2. Statistics of particle number concentrations measured during NPF event days and non-event days. Unit: cm^{-3} for N_{total}, N_{acu}, N_{Aitken} and N_{nuc}.

	Parameters	Average	Median	95th percentile	S.D.	No. of data
NPF event days	N_{total}	9.44×10^3	6.28×10^3	24.1×10^3	7.87×10^3	264
	N_{acu}	1.30×10^3	1.18×10^3	3.08×10^3	0.94×10^3	264
	N_{Aitken}	5.71×10^3	3.30×10^3	15.7×10^3	5.47×10^3	264
	N_{nuc}	2.43×10^3	1.54×10^3	8.10×10^3	2.53×10^3	264
Non-event days	N_{total}	6.09×10^3	3.77×10^3	17.3×10^3	5.82×10^3	339
	N_{acu}	1.09×10^3	0.68×10^3	3.27×10^3	1.04×10^3	339
	N_{Aitken}	$3.43x10^3$	1.87×10^3	9.83×10^3	3.75×10^3	339
	N_{nuc}	1.58×10^3	1.04×10^3	4.30×10^3	1.75×10^3	339

ACPD
13, 8985–9016, 2013

Table 3. Summary of averaged particle number concentration, growth rate, formation rate, and ozone photolysis measurements for NPF events. Note: start and end time are referred to the period of nucleation mode particles growing through 25 nm which used to calculate the GR.

Event date	Start time	End time	GR ($nm\,h^{-1}$)	J_{10-25} ($cm^{-3}\,s^{-1}$)	N_{total} (cm^{-3})	N_{nuc} (cm^{-3})	O_3 (ppb)	$J(O^{1D})$ ($10^{-5}\,s^{-1}$)	$J(O^{1D})\cdot O_3$ ($ppt\,s^{-1}$)
8 Jul 2012	09:00	10:35	5.9	2.89	18.2×10^3	9.67×10^3	36	3.50	1.26
9 Jul 2012	09:35	10:20	25.5	4.78	27.1×10^3	9.42×10^3	47	3.41	1.60
11 Jul 2012	10:00	11:25	5.0	2.67	23.5×10^3	13.0×10^3	48	3.59	1.72
12 Jul 2012	09:15	10:50	7.6	1.62	17.6×10^3	10.1×10^3	33.5	3.50	1.17
13 Jul 2012	09:00	10:45	5.4	1.36	15.1×10^3	8.85×10^3	32	3.31	1.06
14 Jul 2012	09:00	10:05	8.9	2.34	15.8×10^3	7.90×10^3	30	3.24	0.97
18 Jul 2012	08:55	10:45	4.3	1.59	20.9×10^3	11.4×10^3	27	1.64	0.44
19 Jul 2012	09:00	09:45	10.6	0.63	12.9×10^3	3.54×10^3	49	3.12	1.53
27 Jul 2012	09:00	10:20	3.3	1.48	18.1×10^3	8.47×10^3	26	3.45	0.90

ACPD
13, 8985–9016, 2013

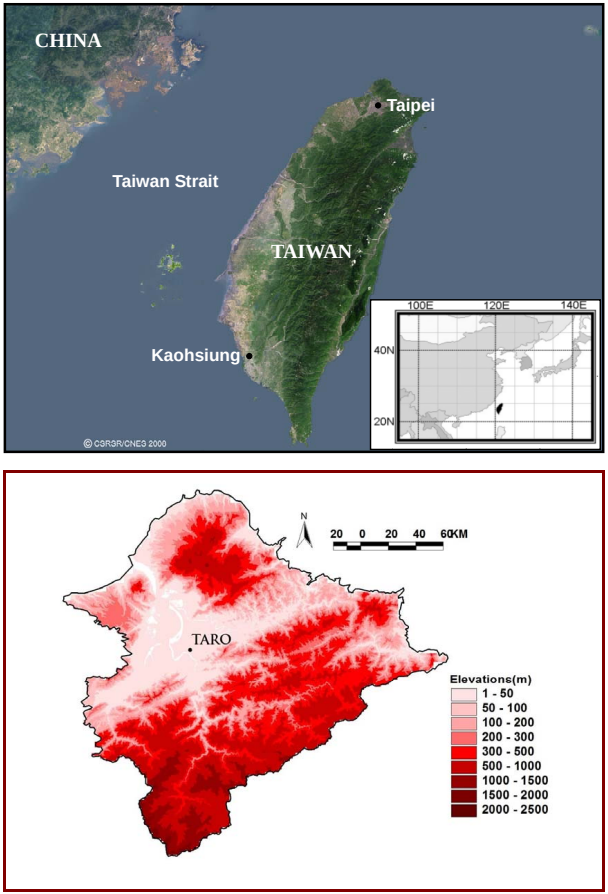

Fig. 1. Geographical locations of Taiwan in East Asia (upper panel) and the Taipei Aerosol and Radiation Observatory (TARO) in the Taipei basin (lower panel).

ACPD
13, 8985–9016, 2013

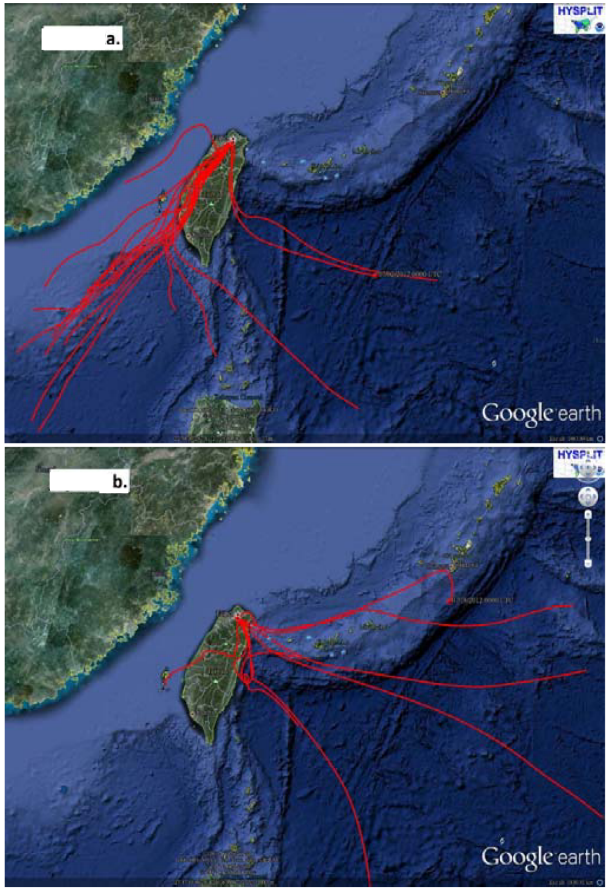

Fig. 2. Daily 72 h backward trajectories calculated for TARO (red dot) during the period of **(a)** 4–19 July and **(b)** 20–27 July of 2012. Trajectories were calculated from 100 m a.g.l. for 08:00 LT each day.

ACPD
13, 8985–9016, 2013

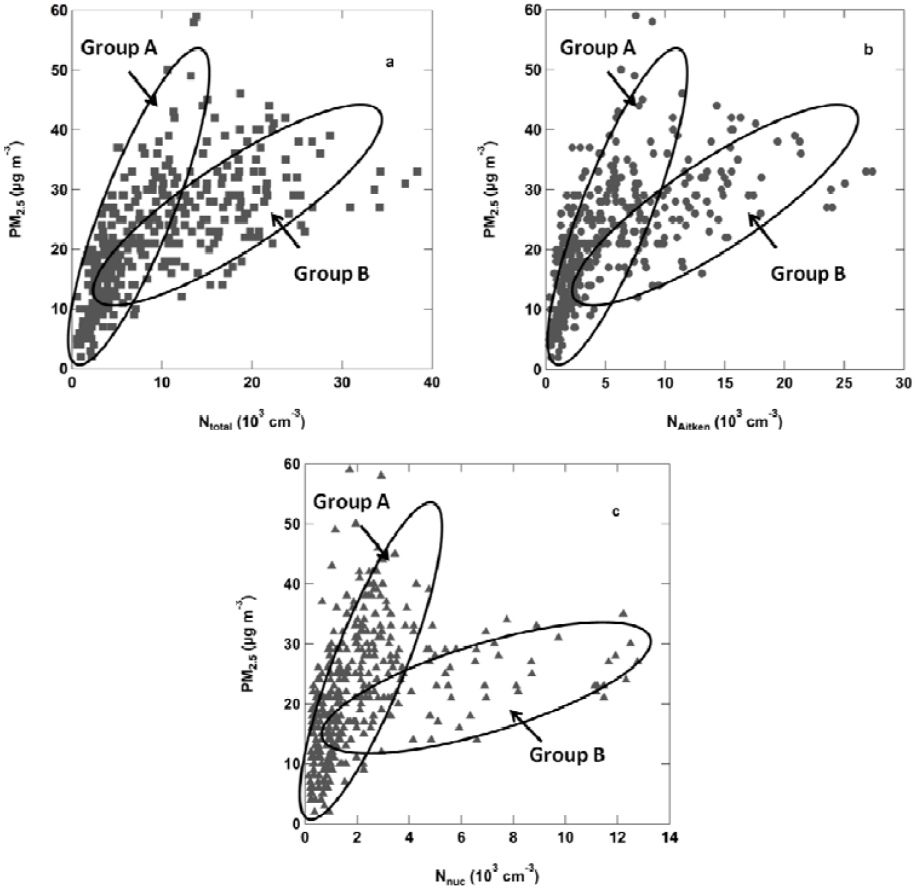

Fig. 3. Scatter plots of number concentrations **(a)** N_{total}, **(b)** N_{Aitken} and **(c)** N_{nuc} against $PM_{2.5}$.

ACPD
13, 8985–9016, 2013

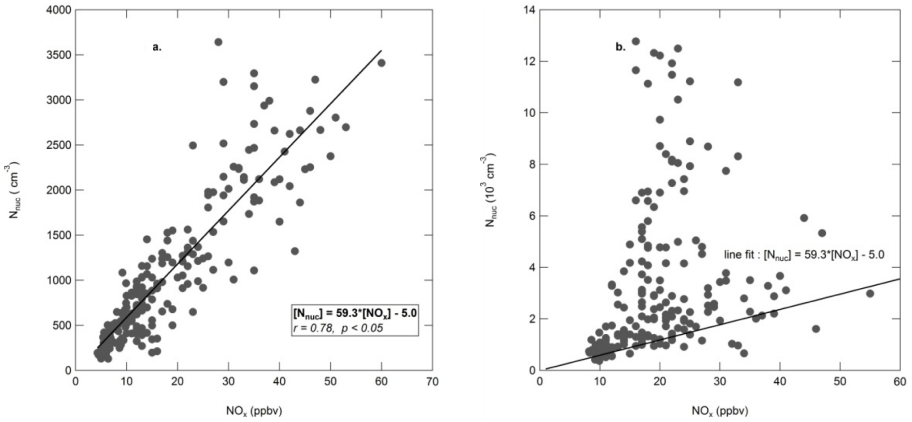

Fig. 4. Scatter plots of number concentrations of nucleation mode particle (N_{nuc}) against mixing ratio of NO_xduring **(a)** nighttime (20:00–03:59) and **(b)** daytime (08:00–15:59). The regression line obtained for nighttime data **(a)** was superposed onto the daytime data **(b)** to indicate the relationship between N_{nuc} and NO_x without disturbance from photochemical reactions.

ACPD
13, 8985–9016, 2013

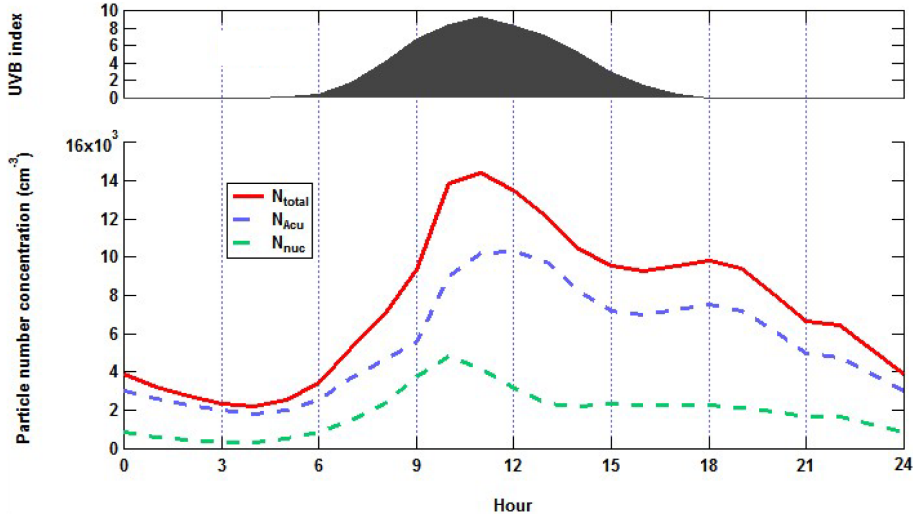

Fig. 5. Diurnal variation of particle number concentrations of total (N_{total}, red solid line), accumulation (N_{acu}, blue dash line), and nucleation (N_{nuc}, green dash line) modes in lower panel, also UVB index in upper panel.

ACPD
13, 8985–9016, 2013

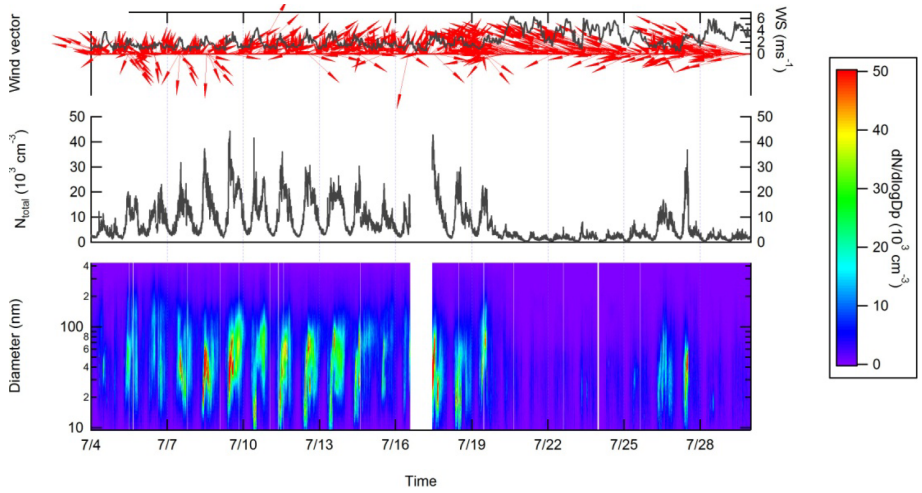

Fig. 6. Time series of measured parameters for summer 2012. From bottom to upper panels are: (i) particle size distribution, (ii) total particle number concentration (N_{total}) and (iii) wind direction (wind vector) and speed (WS).

ACPD
13, 8985–9016, 2013

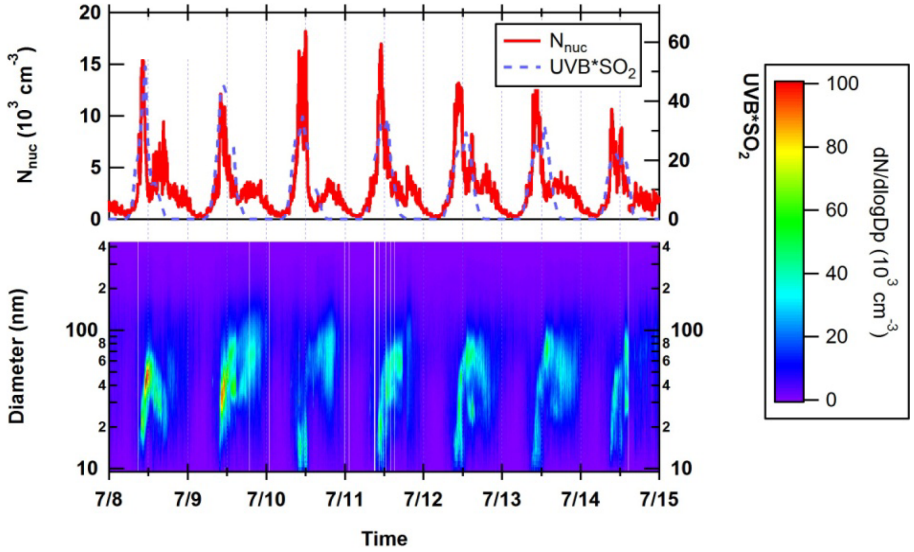

Fig. 7. Time series of particle size distribution (lower panel); and number concentration of nucleation mode (N_{nuc}) and UVB $\cdot$ SO_2 (upper panel) for 8–14 July 2012.

ACPD
13, 8985–9016, 2013

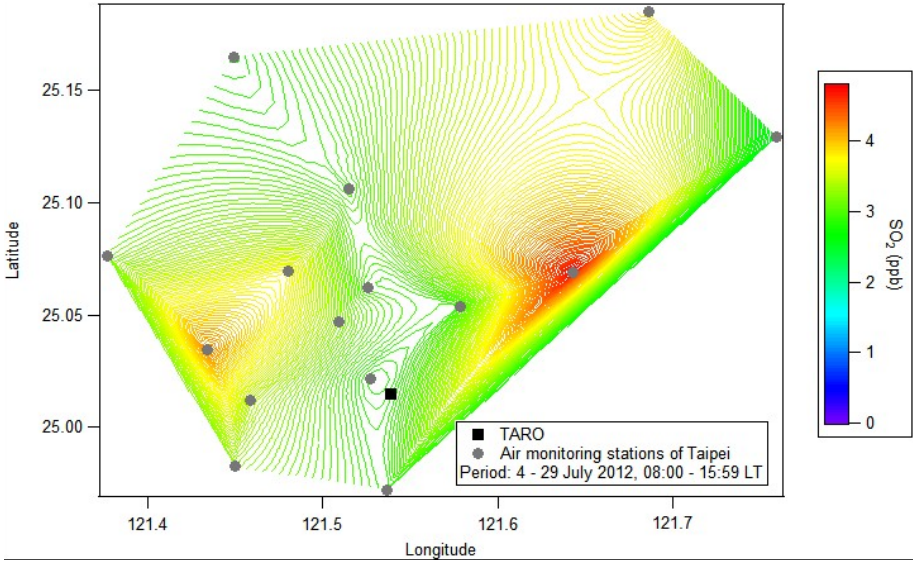

Fig. 8. Mean SO_2 mixing ratio of Taipei region measured during 4–29 July 2012. Square dot: TARO, and circle dots: air-quality monitoring stations of Taiwan EPA.

ACPD
13, 8985–9016, 2013

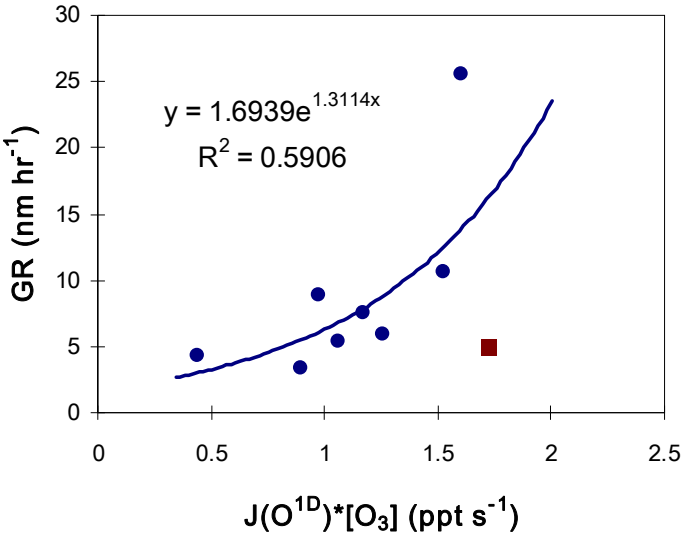

Fig. 9. Correlation between the growth rate of nucleation mode particles and the photolysis of ozone for the NPF events identified in this study. Photolysis of ozone is assumed the dominant term in the production of OH radicals and, thereby, used as an indicator of photochemical production of semi-volatile species that in turn condensed on the preexisting particles and contributed to the particle growth. The square denotes the outlier data point for 11 July 2012 that was excluded from the curve-fitting analysis (see main-text for details).

ACPD
13, 8985–9016, 2013

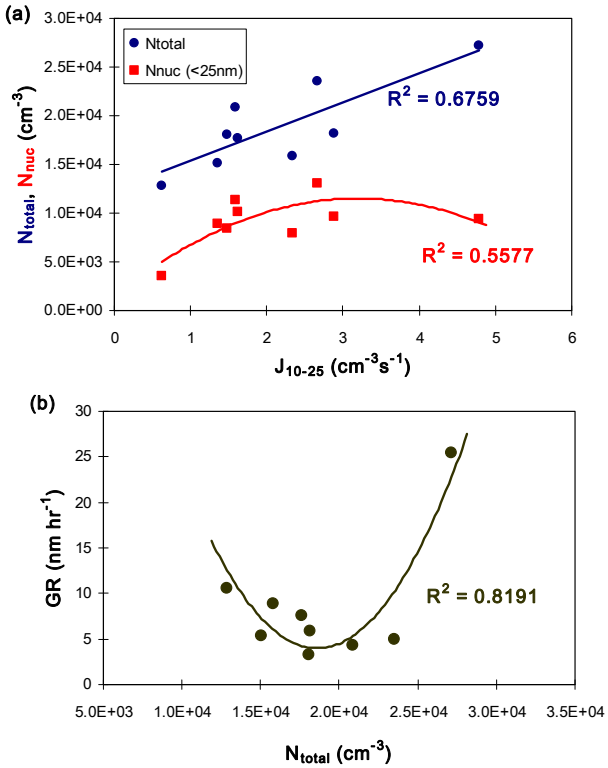

Fig. 10. (a) Responses of the total and nucleation mode particle number concentrations (N_{total} and N_{nuc}) to the changes in the nucleation mode particle formation rate (J_{10-25}), and **(b)** Dependence of particle growth rate (GR) to the total particle number concentration (N_{total}) during the NPF episodes analyzed in this study. The dependencies are illustrated with linear regression (N_{total} vs. J_{10-25}) or quadratic curve-fitting (N_{nuc} vs. J_{10-25} and GR vs. N_{total}).

ACPD
13, 8985–9016, 2013